IN VIVO MEASURES OF COCHLEAR LENGTH AND INSERTION DEPTH OF NUCLEUS COCHLEAR IMPLANT ELECTRODE ARRAYS

DARLENE R. KETTEN, PHD
BOSTON, MASSACHUSETTS

MARGARET W. SKINNER, PHD
ST LOUIS, MISSOURI

GE WANG, PHD
IOWA CITY, IOWA

MICHAEL W. VANNIER, MD
IOWA CITY, IOWA

GEORGE A. GATES, MD
SEATTLE, WASHINGTON

J. GAIL NEELY, MD
ST LOUIS, MISSOURI

Three-dimensional cochlear canal lengths, electrode array intracochlear insertion depths, and characteristic frequency ranges were estimated for 20 Nucleus implant recipients on the basis of in vivo computed tomography (CT) scans. Ultra-high resolution images were reconstructed from spiral CT data with 0.1-mm slicing and expanded attenuation scales. Canal length estimates (mean 33.01 mm; SD 2.31) were consistent with previous findings for normal human temporal bones. Intracochlear array insertion depths estimated by 3-dimensional (3-D) spiral calculations (mean 20.19 mm; SD 2.86) and by a computerized array tracking algorithm (mean 20.36 mm; SD 2.66) were not significantly different. Estimates from surgical observations were significantly longer (mean 21.03 mm; SD 2.31) because array compressions were not detectable. Characteristic frequencies at apical electrodes estimated from Greenwood's equations ranged from 387 Hz to 2,596 Hz. The results show that significant variations in cochlear anatomy and array distribution among implant patients that may impact implant performance can be reliably detected and quantified by using in vivo high-resolution CT and 3-D reconstructions.

KEY WORDS — cochlear canal length, cochlear implant, electrode array, inner ear morphometry, inner ear prosthesis, three-dimensional reconstruction.

INTRODUCTION

This paper represents the first in vivo study of 3-dimensional (3-D) cochlear morphometry and implant array relationships in Nucleus implant recipients. The research was prompted by a need for a better understanding of why and how electrode placements vary among implant recipients. It also served to test the feasibility of 3-D measures of electrode distributions in vivo.

Accurate measures of the intracochlear "fit" of implanted multi-electrode arrays for individual patients are essential for understanding variability in speech recognition,[1,2] improving array insertion procedures,[3] and designing new electrode configurations to more effectively stimulate each patient's residual neural population.[4] Clinically, knowledge of insertion depth, interelectrode separations, and precise location of array distortions can provide an objective base for determining whether changes in performance are related to shifts in array position and for selecting electrode stimulation paradigms, pairing modes, and frequency band assignments in each patient's speech processor program.[5,6] Experimentally, knowledge of intracochlear distributions of electrodes is essential for correlating electrical field model results with psychophysical data, particularly threshold differences, growth of loudness, pitch, and temporal discrimination at suprathreshold levels on each electrode.[4-6]

At present, implanted electrode bandwidths are generally assigned arbitrarily. In two earlier studies,[7,8] a preliminary attempt was made to approximate individual differences in characteristic frequencies associated with the array. In these studies, an average human cochlear length and frequency distribution were assumed. Cochlear penetration of the array was estimated from the surgeon's report of the number of electrodes or stiffening rings placed inside the cochlea. Even with these relatively nonspecific measures, speech perception improved for some patients if bandwidth assignments were based on the average characteristic frequency for the estimated

From the Department of Otology and Laryngology, Harvard Medical School, Boston, Massachusetts (Ketten), the Department of Otolaryngology–Head and Neck Surgery, Washington University School of Medicine, St Louis, Missouri (Skinner, Neely), the Department of Radiology, The University of Iowa, Iowa City, Iowa (Wang, Vannier), and the Department of Otolaryngology–Head and Neck Surgery and the Virginia Merrill Bloedel Hearing Research Center, University of Washington, Seattle, Washington (Gates). Supported by grants from the National Institutes of Health/National Institute on Deafness and Other Communication Disorders (DC00581, DC00361, and DC02798), Siemens Medical Systems, Inc, and the Whitaker Foundation (Biomedical Engineering Program).

CORRESPONDENCE — Darlene R. Ketten, PhD, Harvard Medical School, Massachusetts Eye and Ear Infirmary, 243 Charles St, Boston, MA 02114.

array insertion depth.

Surgical observation is the most common method currently used to estimate electrode insertion.[9] However, substantial anatomic and neural variations exist in patient inner ears that may affect intracochlear penetration and frequency distributions.[10-17] External observations cannot accurately measure intracochlear differences in array placement, and patients who have equal components inserted do not necessarily have equal intracochlear coverage or frequency distributions.[9,11,18] To optimize frequency boundary assignments, *patient-specific* knowledge about intracochlear electrode distributions and their correspondent frequencies is required.

Precise determination of intracochlear array position is important because humans, like other mammals, have tonotopically organized cochleae. Von Békésy's[19] work on membrane elasticity and frequency-position measures showed frequency response characteristics in all mammals are similarly and exponentially distributed along the basilar membrane, with highest frequencies encoded at the base and lowest at the apex. Greenwood's equations,[20-23] which were derived from von Békésy's measures, are a commonly accepted method for estimating characteristic frequency-versus-length relationships in different species.[24] Greenwood's conclusion, based on the fact that most mammalian basilar membranes scale isometrically with the average human membrane, was that frequency distributions could be predicted for any ear based on one variable, length.[20,22] In actuality, stiffness, not length, is the primary structural correlate of inner ear frequency response characteristics.[19,25] Basilar membrane thickness and width are the principal variables affecting membrane stiffness; however, for regularly configured mammalian ears like those that Greenwood used in formulating his equations, thickness and width covary with length.[26-28] For these ears, which have basilar membranes that are isomorphic with those of humans, Greenwood's equations reliably predict characteristic frequency distributions from knowledge of length alone.[24,27]

Greenwood's formulae have also been used to analyze human frequency-length distributions.[7,8,24,29,30] The substantial variation found in human cochlear lengths implies that significant differences may exist in intracochlear frequency distributions.[10,14,22] For implant recipients, understanding interindividual frequency variations may be crucial. Greenwood's formulae are theoretically applicable at the individual level and provide a venue not only for estimating but, equally important, for testing characteristic frequency distributions of auditory fibers at different electrode positions in each patient. However, in order to employ Greenwood's equations, it is necessary to have reliable measures of both cochlear length and intracochlear position of the array.

Postoperative radiographs can provide more precise measures of a patient's intracochlear electrode placement than intraoperative observations.[29,30] Marsh et al[29] found a significantly higher correlation between individual sentence recognition scores and array position when implanted length was estimated from modified Stenver's view plain film X-rays ($r = .59$; $p < .006$) than when it was estimated from surgical observations ($r = .33$; $p < .15$). Cohen et al[30] carried the approach of Marsh et al a step further by producing a template for estimating the angular spread of the array. They noted that lines of equal length will cover different percentages of a family of curves that have the same curvature but different radii. Therefore, they reasoned, given that most human ears have similar curvatures but different cochlear canal radii, patient array insertion depth can be fairly well described in terms of the angular distribution of the array. Cohen et al[30] measured the angular position of the most apical electrode in 2-dimensional (2-D) X-ray projections with respect to the entry point and estimated characteristic frequency at the tip of the array by comparing this position to an angle-average human frequency distribution derived from Bredberg's[12] data relating angle to length and Greenwood's[22] function relating frequency to length. These 2-D approaches provide good first-order approximations of electrode array insertion lengths, but because overlying structures obscure fine detail, they may not provide sufficient information about cochlear length or intracanal array position to allow detailed analysis of interpatient differences or frequency-position relationships for specific electrodes.

Computed tomography (CT) provides high-resolution images of both the implanted array and the cochlea and has the advantage of providing aligned, sectional data that facilitate 3-D reconstruction and cochlear measurements.[31-35] Spiral CT scanning, a recent advance that employs continuous, simultaneous source rotation, patient translation, and data acquisition, has an in-plane resolution equivalent to that of conventional CT, but provides substantially better longitudinal resolution and allows retrospective slice reconstruction at multiple thicknesses from a single CT data set.[36-38] Isotropic voxels on the order of 100 μm are clinically feasible, and Skinner et al[33] demonstrated that intracochlear electrode positions could be determined with a resolution of ±300 μm by using ultra-high resolution, submillimeter spiral scan images. With spiral techniques, cochlear and

TABLE 1. PATIENT PROFILES

Patient	*Sex*	*Age at Implantation*	*Ear*	*Bands Inserted*	*History*
1	F	70	R	28	Progressive after measles or mumps
2	M	35	L	25	Progressive after maternal rubella
3	F	74	R	29	Unknown; reimplantation for failed Nucleus device
4	F	52	R	28	Otosclerosis
5	F	74	L	28	Genetic; otosclerosis
6	M	76	R	22	Vascular accident; diabetes
7	F	84	L	32	Unknown
8	M	79	R	28	Otosclerosis
9	F	72	R	29	Unknown
10	M	53	R	22	Unknown; sudden onset; noise exposure
11	F	36	R	27	Unknown; degenerative cerebellar disease
12	M	69	L	32	Otosclerosis
13	F	47	L	26	Progressive after meningitis
14	F	39	L	24	Right ear deaf at birth; left ear progressive loss detected in infancy
15	F	72	R	30	Progressive mixed hearing loss; sudden onset of deafness in left ear possibly owing to viral infection
16	M	61	R	32	Right ear following high fever; left ear unknown
17	F	60	L	27	Progressive following radical bilateral mastoidectomy for chronic otitis media
18	M	59	R	32	Progressive after measles or mumps; noise exposure; Meniere's disease
19	F	75	R	29	Progressive after measles; bilateral radical mastoidectomy for chronic otitis; Nucleus replacement for 3M/House device
20	F	82	R	28	Otosclerosis; noise exposure

array detail can be measured rapidly in vivo at a resolution sufficient for calculating individual frequency distributions. Equally important, with high-resolution, rotatable 3-D reconstructions, array positions can be accurately compared among patients and, over time, within each patient.

In this study, we extended the work by Skinner et al[33] and combined submillimeter in vivo imaging and 3-D reconstruction with Greenwood's formulae. Two algorithms were employed to estimate array insertion depths and cochlear lengths in 20 patient ears: 1) 3-D calculations of length based on individual spiral fits to 2-D CT midmodiolar images, and 2) automated computerized calculations from 3-D visualizations of the array obtained by segmenting for electrode attenuation properties. Length estimates from both forms of CT analyses were then compared with estimates based on the surgeon's observations for each patient. Our primary goal was to determine the highest practical resolution of array position and cochlear variability afforded by these techniques for in vivo data. In light of the imaging results, we extended our analyses to theoretical predictions of frequency distributions for individual implant recipients, which we report here as preliminary results.

METHODS

Patient Scanning. Twenty adult patients implanted with Nucleus Cochlear Implant Systems at Washington University School of Medicine between March 1992 and June 1995 were imaged with a spiral scanning protocol. The study population included 13 female and 7 male patients implanted between the ages of 35 and 84. Deafness was attributed to a wide range of causes that are representative of the major known causes for profound hearing loss. Patient profiles are summarized in Table 1.

Preoperative and postoperative scans were obtained with a Siemens Somatom PLUS S CT scanner using a conventional spiral temporal bone protocol with 1-mm detector collimation at 1-mm/s table feeds. All images were reconstructed with an ultra-high kernel and 512 matrix. In preoperative images, a conventional 12-bit attenuation scale was used. For postoperative scans, a 10-fold expansion of the attenuation scale was applied to the data to improve discrimination of metallic components of the electrode array. Siemens experimental software was used also to reconstruct images at 100-μm slice intervals for selected preoperative data and for all postoperative scans. With these parameters, the maximum in-plane resolution is 0.35 mm at 2% of the modulation transfer function.

Preoperative spiral CT data were available for 18 patients, including 2 candidates for reimplantation (Table 1). Postoperative spiral CT data were obtained

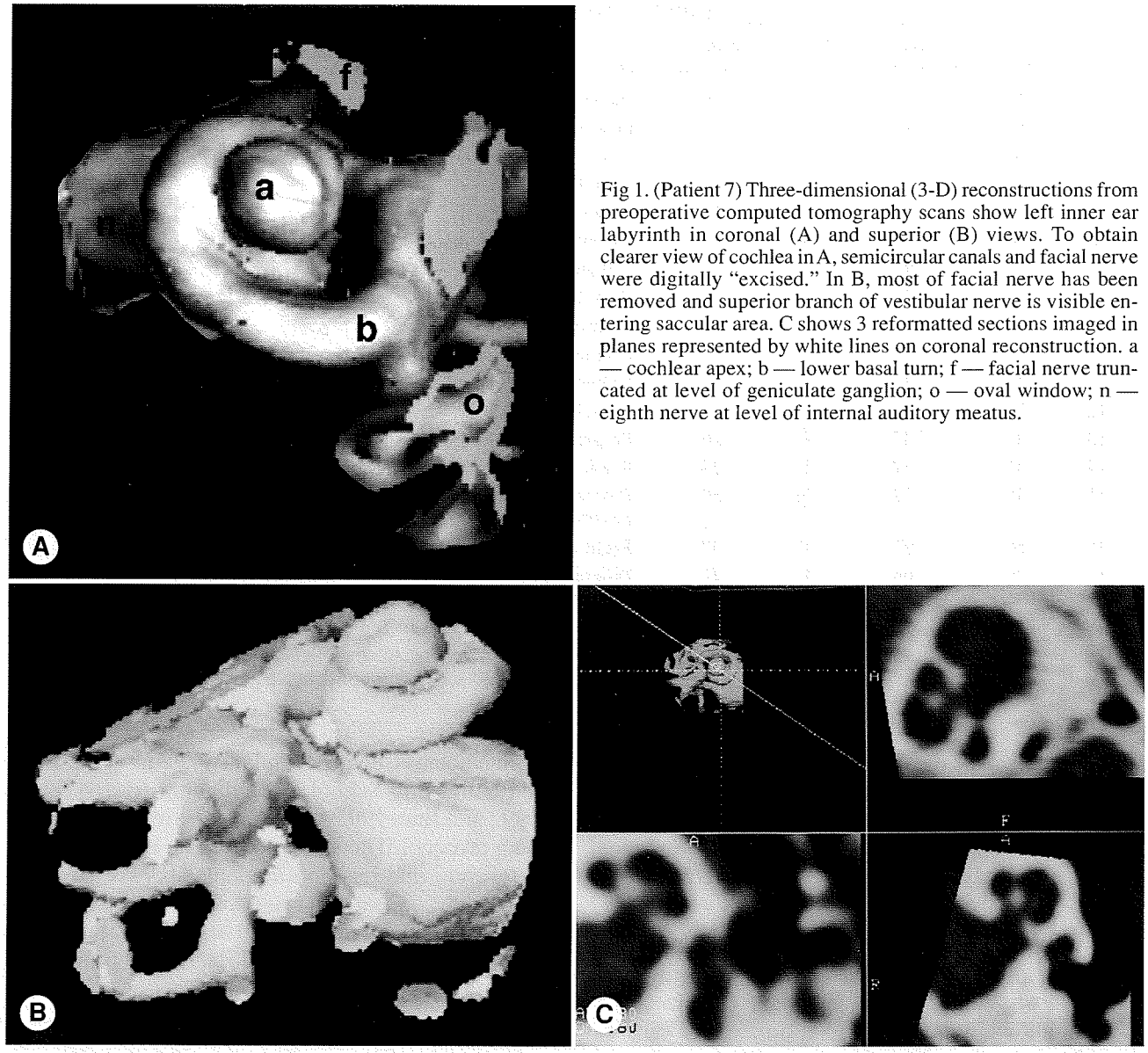

Fig 1. (Patient 7) Three-dimensional (3-D) reconstructions from preoperative computed tomography scans show left inner ear labyrinth in coronal (A) and superior (B) views. To obtain clearer view of cochlea in A, semicircular canals and facial nerve were digitally "excised." In B, most of facial nerve has been removed and superior branch of vestibular nerve is visible entering saccular area. C shows 3 reformatted sections imaged in planes represented by white lines on coronal reconstruction. a — cochlear apex; b — lower basal turn; f — facial nerve truncated at level of geniculate ganglion; o — oval window; n — eighth nerve at level of internal auditory meatus.

from all 20 patients 4 to 5 weeks after implantation. Surgical reports indicated all patients had 22 electrodes inserted into the scala tympani. Stiffening rings inserted varied from 0 to 10.

Cochlear Canal Length Estimates. For accurate length calculations, it is necessary to obtain a midmodiolar projection. Cochlear tilt varies among individuals; however, paramodiolar sections can be obtained by matching the scanner gantry tilt to a line drawn from the petrous apex, ie, the superior margin of the petrous bone on the topogram, to the inferior margin of the zygomatic arch.[39] For these cases, measurements were made from the original 2-D images. For patients whose scans were performed without matching gantry tilt to the cochlear axis, measurements were taken from paramodiolar images reformatted from 3-D reconstructions of the inner ear labyrinth segmented for intralabyrinthine attenuations by means of Siemens on-line software (Fig 1).

Cochlear measurements were obtained from hard copies of CT images with Mitutoyo steel calipers (model 5056470; ±0.02-mm repeat resolution). Measurements were repeated at 2× to 7× magnification on an Olympus model SZH10 stereomicroscope with a 55-mm maximal field of view. For scope measurements, a 100-division eyepiece reticule was calibrated at each magnification with a 2-mm graticule with 0.01-mm divisions (Graticules, Ltd, Kent, England). In some cases, scope images were also digitized with a Sony 3CCD video system and the measurements were repeated with NIH Image (version 1.58) on a Macintosh Quadra 840AV.

Because the basilar membrane cannot be detected

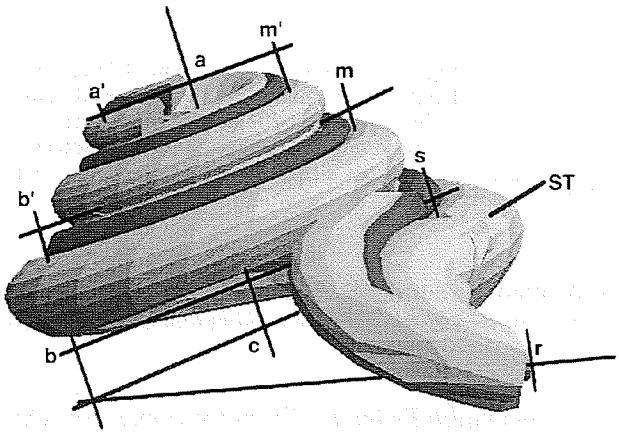

Fig 2. Scaled schematic of human cochlea shows intracanal locations used to determine cochlear radii and height for 3-D spiral calculations. Diameters listed in Table 2 are sum of radii. a'- m' — apical diameter; m-b — middle diameter; b-s — basal diameter; a-c — axial height; r-s — hook length; ST — scala tympani. (3-D representation, copyright D. R. Ketten, 1990).

in CT scans, cochlear length was defined as the length of the centroid of the fluid space of the cochlear labyrinth resolvable in the CT images. This arc is approximately equal to the juncture of the basilar membrane and the inner osseous lamina. The radius of each half turn and the axial height of the cochlear canal were measured from the midmodiolar images. The cochlear radii are the lengths of lines subtended at right angles from the modiolar axis to the centroid of the canal[26,33] (Fig 2). Measurements were repeated until 3 were within 0.05 mm. The average of these 3 was used as the final number for each cochlear parameter (Table 2) used in the length calculations.

Canal lengths were calculated by Ketten's[26] method for estimating 3-D cochlear lengths for Archimedean and equi-angular spirals from the 2-D parameters of the radius at angular displacement θ (in radians); *a*, a constant related to the ratio of the radii (Fig 3); and *h*, axial height. In this case, *a* was calculated for each patient from measures of cochlear turn radii (Table 2). The Archimedean spiral is one of two regular curves commonly used to model mammalian cochleae,[26] and it provides the closest fit of any regular curve for the midline of human cochlear canals. Our principal assumption is therefore that the cochlear spiral in all patients has a common configuration but that each spiral length is patient-specific and can be calculated by determining the actual radii and the spiral constants dictated by that patient's turn dimensions.

The hook region is a small component of cochlear length, but because it was not clear that a single spline fit would provide a good approximation for all hook

TABLE 2. COCHLEAR MEASUREMENTS

	Cochlear Canal Measurements (mm)			*Calculated Values*		
Patient	*Axial Height*	*Basal Diameter*	*Middle Diameter*	*Apical Diameter (mm)*	*Spiral Constant a*	*Cochlear Length (mm)*
1	3.30	8.91	3.90	1.59	0.25	33.99
2	3.20	8.00	3.60	1.60	0.23	32.18
3	1.93	8.00	4.20	1.80	0.25	34.73
4	2.38	8.06	4.74	1.12	0.23	31.51
5	3.33	8.33	3.75	1.67	0.27	36.17
6	4.00	7.50	4.00	2.00	0.26	35.14
7	2.32	7.25	4.12	1.36	0.26	34.98
8	2.70	7.75	5.30	1.89	0.28	37.45
9	2.32	7.87	3.80	1.65	0.24	32.67
10	2.78	9.16	4.57	1.28	0.25	33.67
11	2.54	7.91	3.73	1.22	0.21	29.73
12	2.97	7.82	4.29	1.18	0.25	34.09
13	3.25	7.45	4.76	1.38	0.24	32.54
14	3.15	8.10	5.56	1.47	0.26	35.74
15	2.10	7.43	3.86	1.39	0.22	30.51
16	2.31	7.54	4.15	1.12	0.21	29.51
17	2.18	7.08	4.03	1.18	0.21	29.07
18	2.68	8.00	4.40	1.32	0.23	32.07
19	2.74	8.47	3.80	1.39	0.23	31.81
20	2.81	7.45	4.80	1.67	0.24	32.61
Mean	2.75	7.91	4.27	1.46	0.24	33.01
SD	0.52	0.53	0.54	0.26	0.02	2.31
Median	2.72	7.89	4.14	1.39	0.24	32.64

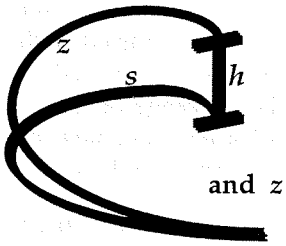

$$\text{For } r = a\theta$$

$$s = \int_{\theta_0}^{\theta_n} \sqrt{r^2 + \left(\frac{dr}{d\theta}\right)^2}\, d\theta$$

$$\text{and } z = \sqrt{\left\{\frac{a}{2}\left[\left(\theta\sqrt{\theta^2+1}\right) + Ln\left(\theta + \sqrt{\theta^2+1}\right)\right]\right\}^2 + h^2}$$

Fig 3. Formulae for estimating 3-D cochlear lengths for Archimedean spiral approximation of human cochlear midcanal spiral path. r — radius at angular displacement θ in radians, a — constant that dictates spiral size, h — axial height.

curvatures, hook anatomy was measured directly in each patient from reformatted projections that approximated the midline of the canal throughout the hook region. This number was added to the primary cochlear canal length calculated from the equations in Fig 3 to obtain each patient's total preoperative cochlear canal length (Tables 2 and 3).

Electrode Array Insertion Depth Estimates. Three methods were used to estimate implant array insertion depth (Table 4): 1) intraoperative reports from the surgical team (S); 2) array length calculations from CT data using Ketten's spiral algorithm (K); and 3) automated tracking of CT reconstructions of the array using Wang's "unwrapping" method (W). All array length assessments by Ketten and Wang were made independently and without knowledge of patient performance data or surgical observations on any patient.

Array Length Estimates From Intraoperative Observations. Implantations of patients in this study were performed by 2 surgeons with different criteria for determining whether a stiffening ring entered the cochlea. For patients 1 through 13, lengths were calculated by simply multiplying the number of electrodes and rings reported inserted by the surgeon (Table 1) times the manufacturer's specifications for electrode and stiffening ring length (0.300 mm) plus interelectrode distance (0.450 mm). For patients 14 through 20, 0.300 mm was added to each length calculation to compensate for an average 1-ring length

TABLE 3. CALCULATED COCHLEAR CANAL LENGTH, PERCENTAGE OCCUPIED BY IMPLANTED ARRAY, AND ESTIMATED CHARACTERISTIC FREQUENCIES

Patient	Cochlear Length (mm)	Array Length (mm)	Array/ Cochlear Length	Frequency at Apex (Hz)		Frequency at Base (Hz)		Frequency at Apical Electrode (Hz)	
				35 mm	33 mm	35 mm	33 mm	35 mm	33 mm
1	33.99	21.64	0.64	22	19	21,921	19,499	862	766
2	32.18	18.72	0.58	24	22	24,455	21,753	1,307	1,163
3	34.73	20.29	0.58	21	19	20,995	18,675	1,106	984
4	31.51	19.91	0.63	25	23	25,504	22,687	1,031	917
5	36.17	21.24	0.59	19	17	19,366	17,227	1,003	893
6	35.14	16.47	0.47	20	18	20,515	18,248	1,998	1,778
7	34.98	23.99	0.69	21	18	20,695	18,408	611	543
8	37.45	21.19	0.57	18	16	18,063	16,068	1,052	936
9	32.67	20.70	0.63	24	21	23,730	21,109	949	844
10	33.67	15.66	0.47	22	20	22,349	19,880	2,215	1,970
11	29.73	13.68	0.46	29	25	28,651	25,486	2,919	2,596
12	34.09	23.33	0.68	22	19	21,798	19,390	648	577
13	32.54	18.05	0.55	24	21	23,915	21,273	1,481	1,317
14	35.74	18.24	0.51	20	18	19,830	17,639	1,554	1,382
15	30.51	22.46	0.74	27	24	27,216	24,209	588	523
16	29.51	23.33	0.79	29	26	29,088	25,874	435	387
17	29.07	18.22	0.63	30	27	29,975	26,663	1,247	1,110
18	32.07	24.46	0.76	25	22	24,625	21,904	447	397
19	31.81	21.63	0.68	25	22	25,032	22,266	765	680
20	32.61	20.67	0.63	24	21	23,824	21,192	951	846
Mean	33.01	20.19	0.61	24	21	23,577	20,973	1,158	1,030
SD	2.31	2.86	0.09	3	3	3,341	2,972	629	559
Minimum	29.07	13.68	0.46	18	16	18,063	16,068	435	387
Maximum	37.45	24.46	0.79	30	27	29,975	26,663	2,919	2,596
Median	32.64	20.69	0.63	24	21	23,777	21,150	1,017	905

TABLE 4. INSERTION DEPTH OF ELECTRODE ARRAY

	Array Insertion Depth Estimates (mm)			*Differences (mm)*		
Patient	*K*	*W*	*S*	*K – W*	*S – K*	*S – W*
1	21.64	20.77	21.00	0.87	–0.64	0.23
2	18.72	18.56	18.75	0.16	0.03	0.19
3	20.29	21.66	21.75	–1.37	1.46	0.09
4	19.91	19.79	21.00	0.12	1.09	1.21
5	21.24	21.36	21.00	–0.12	–0.24	–0.36
6	16.47	18.34	16.50	–1.87	0.03	–1.84
7	23.99	22.79	24.00	1.20	–0.01	1.21
8	21.19	20.78	21.00	0.41	–0.19	0.22
9	20.70	19.56	21.75	1.14	1.05	2.19
10	15.66	15.35	16.50	0.31	0.84	1.15
11	13.68	14.10	20.25	–0.42	6.57	6.15
12	23.33	23.70	24.00	–0.37	0.67	0.30
13	18.05	18.76	19.50	–0.71	1.45	0.74
14	18.24	18.37	18.30	–0.13	0.06	–0.07
15	22.46	23.28	22.80	–0.82	0.34	–0.48
16	23.33	22.98	24.30	0.35	0.97	1.32
17	18.22	18.91	20.55	–0.69	2.33	1.64
18	24.46	23.41	24.30	1.05	–0.16	0.89
19	21.63	22.97	22.05	–1.34	0.42	–0.92
20	20.67	21.83	21.30	–1.16	0.63	–0.53
Mean	20.19	20.36	21.03	–0.17	0.84	0.67
SD	2.86	2.66	2.31	0.89	1.53	1.60
Median	20.69	20.78	21.00	–0.13	0.53	0.27

K — estimates from computed tomographic and spiral calculations by Ketten; W — estimates from tracking and unwrapping algorithm by Wang; S — estimates from surgeon's observations.

difference that would have resulted from the reports of the second surgeon, who had more conservative criteria for reporting components as intracochlear.

Array Length Estimates From Spiral Calculations. Insertion depths of the arrays were calculated from postoperative CT scans according to the procedures described for preoperative canal length. However, for array lengths, it was decided to estimate "functional" canal penetration rather than total inserted array length. In several patients, bends or twists that decreased the cochlear penetration of the array were clearly visible in the postoperative scans (Table 5 and Figs 4 and 5). Further, in some patients, the array entry point bypassed the hook; in others, the hook region was obliterated. Calculating the total length of the array, including the curvature of the distortions in the array, would have overestimated the array's functional coverage of the cochlea or misrepresented its relative position along the canal. An insertion length that is related to the length of the canal covered by the array would more accurately represent the "functional" insertion depth.

Therefore, insertion lengths were calculated by locating the cochlear entry point of the array and the intracochlear position of the apical-most electrode and calculating the arc length covered by the array between those two points. Array entry and end points were determined by visually comparing preoperative and postoperative images. Because the "bloom" created by partial volume averaging visually obscures the apical electrode position (see Fig 5 and Discussion), array tip positions were determined by profiling the tip region to locate attenuations (approximately 20,000 Hounsfield units [HU]) consistent with solid electrode bands. For some cases, it was helpful also to reformat and compare three orthogonal 2-D slices at different positions by using the array's 3-D reconstruction as a guide (Fig 4).

The rotations, radii, and height differences between the entry and end points were used to calculate the functional spiral path length of the array. As a check on the calculations, the length of the canal extending from the array tip to the cochlear apex and the length of any basal, unimplanted regions of the canal were also calculated. These lengths were added to the array path length estimate, and the totals were compared with the preoperative canal lengths. There were no significant differences between the 2 totals for any patient.

Array Length Estimates From Computerized Tracking and Unwrapping. The X-ray attenuation coefficient for platinum is approximately 20,000 HU;

TABLE 5. QUALITATIVE ASSESSMENT OF ELECTRODE PATHS IN COCHLEA-ARRAY INTERACTIONS

Patient	*Entry*	*Lower Basal to Mid-basal Turn*	*Upper Basal Turn to Array Tip*	*Array Turns*
1	Straight entry; track crosses hook	Entry approximately mid-basal	No torsion of array; well-centered in canal	1.00
2	Straight entry	Slight kink	Against outer wall	0.75
3	Straight entry	Modiolus degraded; array impacts outer wall early in turn; distinct bump 6.2 mm from round window	Array against outer wall most of its length; minor scala tympani to scala media excursion	1.00
4	Straight drill track beginning just inferior to round window	Array tunnels through cochlear canal that is partly occluded by fibrous and bony tissues	Moderate twist	1.00
5	Entry beyond lower basal turn	Array impacts outer wall at first bend	Distinct scala tympani to scala vestibuli curve with deep kink and recurve of array	<1.00
6	Doubling of array at entry	Deep kink; multiple twists	Complete recurve of array at tip	<0.75
7	Dip in array curvature after entry	Bony spheroids associated with array	Fibrous and bony sheath surrounds array	1.25
8	Entry near round window	Fibrous tissue filling basal turn	Fibrous tissue; distinct scala tympani to scala vestibuli excursion of array	1.00
9	Entry appears to follow hook	Bony and fibrous tissue associated with array; distinct shift into scala media 5.2 mm after hook	Well-defined curve from scala tympani to scala vestibuli at upper basal turn	1.00
10			Tip clearly located in scala media or scala vestibuli	<0.75
11	Drill entry 0.5 mm inferior to round window; nearly parallel to basal turn	Repeated compressions of array; fibrous occlusions noted preoperatively now largely bone; array impacts outer wall in first quarter turn	Array heavily compressed; insertion probably compromised by narrow canals and occlusions evident in preoperative scans	0.50
12		Extensive soft tissue; double twist	Extensive soft tissue depositions	<1.00
13		Moderate crimping	Clear arc of array into scala vestibuli	0.75
14		Array twisted but centered in scala tympani	Impacts outer wall but remains in scala tympani	0.75
15	Drill out 5 mm inferior to basal turn	Array centered in cochleostomy; enters basal turn just beyond hook; kink just past entry	Remains in scala tympani	>1.50
16	Extensive soft tissue in drill track	Heavy kink in lower basal turn		>1.50
17	Straight entry	Fibrous and bony tissue filling canal		<1.00
18		Array at outer wall 7 mm from round window but remains in scala tympani; fibrous tissue	Canal exceptionally narrow; array tip curves toward modiolar wall	1.00
19	Straight; hook obliterated	Reimplantation surgery removed occlusions and broadened basal turn		1.25
20	Entry obscured by soft and bony tissue	Fibrous and bone blocks throughout basal turn	Array twisted in upper basal turn and sitting against outer wall	<1.00

therefore, the array structure can be readily visualized via simple thresholding (Figs 4 and 5). Multiple reconstructions of the array were surveyed by using the ANALYZE software package[40] to obtain the most representative threshold values (Fig 5). ANALYZE was also used to determine coordinates with a common framework for the cochlear entry point, a second intracochlear point, and the array tip required for the tracking procedure. As described above, electrode sites were determined by sequentially measuring attenuations along the 3-D array track and locating the coincidence of these points in multi-planar reformatted 2-D views. Entry and tip points were reliably chosen with a ±3-pixel repeatability (±0.35 mm). An "unwrapping" program[41] calculated array length based on a sequence of arcs at arbitrary intervals (0.5 mm here) along the central axis of the array. With the cochlear entry as a start-

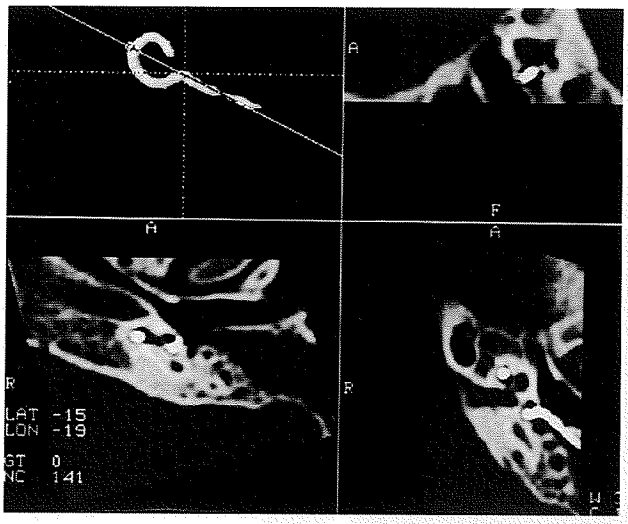

Fig 4. (Patient 2) Upper left panel shows diagonal line bisecting 3-D reconstructed image of electrode array. Entry point is at intersection of this line and patient 2's sharp bend in array. Lower right panel shows 2-dimensional (2-D) image of array entry point viewed from middle ear, from reformatted section at diagonal line in 3-D image. Other lines show planes of section for other 2-D reformatted images used for assessing this patient.

ing point, subsequent positions were estimated along the local direction, based on the center of mass for thresholded structures. This procedure was repeated until the end point was within the 0.5-mm arc length specified. The total array length was computed from the number and sequence of central axis positions and associated local directions between starting and end points.

Calculation of Characteristic Frequencies. Greenwood's equation for calculating frequency distributions along the basilar membrane is $F = A(10^{ax} - k)$ where F is frequency, x is the position in millimeters on the basilar membrane, k is an empirically derived constant, and a is a species-specific constant inversely related to cochlear size. For all ears, ax = 2.1 for 100% length. A is a normalization constant calculated from the human average constant (Ah) and the ratio of the subject basilar membrane length (Ls) versus average human length (Lh): $As = (Ah) \times (Lh/Ls)^2$. Values for the human average derived by Greenwood[20-23] are A = 165.4 and a = 0.06.

To apply Greenwood's formulae at the individual level, a single value for the constant k needed to be assigned and independent values for As calculated from each patient's cochlear length. In previous papers, Greenwood has used values of 0.80, 0.85, 0.88, and 1.0 for k for human cochleae, depending on the criteria for fit.[20-23] A value k = 0.88 was selected for this study because of Greenwood's conclusion that this value achieves the best fit for lower-frequency hearing characteristics in humans.[20,21,24] Greenwood also used an estimate for average cochlear length of 35 mm, but gave no explicit rationale for this choice.[21] Because the mean cochlear canal length of patients in this study differed (33.01 mm), 2 calculations were made for each patient: 1 normalized to 35 mm and the other to 33.01 mm.

RESULTS

Three-Dimensional Cochlear Length. Table 2 shows the axial heights, turn diameters, spiral size constants, and cochlear canal lengths obtained from measurements of preoperative and/or postoperative CT scans for each patient. The greatest percent differences among patients occurred in axial heights (range 1.93 to 4.00 mm). Basal, middle, and apical turn diameters (sum of the radii for the appropriate half turns) ranged from 7.08 to 9.16 mm, 3.60 to 5.56 mm, and 1.12 to 2.00 mm, respectively. Cochlear canal lengths in this group ranged from 29.07 to

Fig 5. (Patient 3) Multiple 3-D reconstructions of implanted Nucleus array produced at different thresholds by using ANALYZE illustrate effects of partial volume averaging and progressive thresholding for differentiating apical electrode from array's SILASTIC® tip (left to right: 4,760, 7,260, and 9,760 Hounsfield units). In left panel, incorporation of partial volume averaging effects at lowest threshold produces artificially thick silhouette of whole array (platinum electrodes, platinum-iridium lead wires, and silicone carrier). At right, tapering of array is evident. Constriction of most apical electrode near tip is clearly visible in comparison to thicker silicone carrier. Apparent disappearance of array parts in some regions is, in sense, other end of spectrum of partial volume effects from blooming; ie, array appears to be discontinuous in areas in which lead wires are present, but their mass is small enough that average attenuation of related pixels is below threshold chosen for reconstruction.

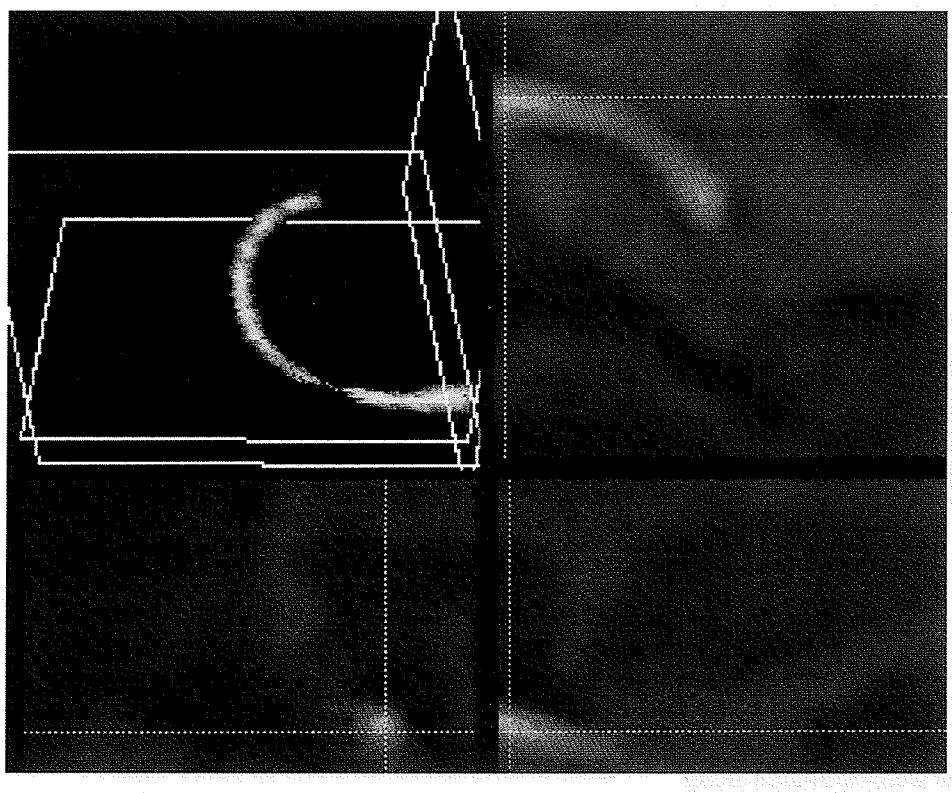

Fig 6. (Patient 11) Implanted array occupies approximately one half turn and has sufficient compressions throughout its length that it appears to be relatively broad, featureless tube in this 3-D representation. This array occupies 46% of patient's cochlear length.

37.45 mm; ie, they differed by as much as 8.38 mm or approximately 25% of the commonly accepted cochlear length norm. This range and variability are large, but are consistent with data obtained from other 3-D analyses of postmortem temporal bones.[11-14] The mean spiral constant for the group, 0.24, can be considered a representative population value for *a* for formulating an Archimedean model of the average human cochlear canal or basilar membrane mid-line spiral.

The mean cochlear length for male patients (33.45

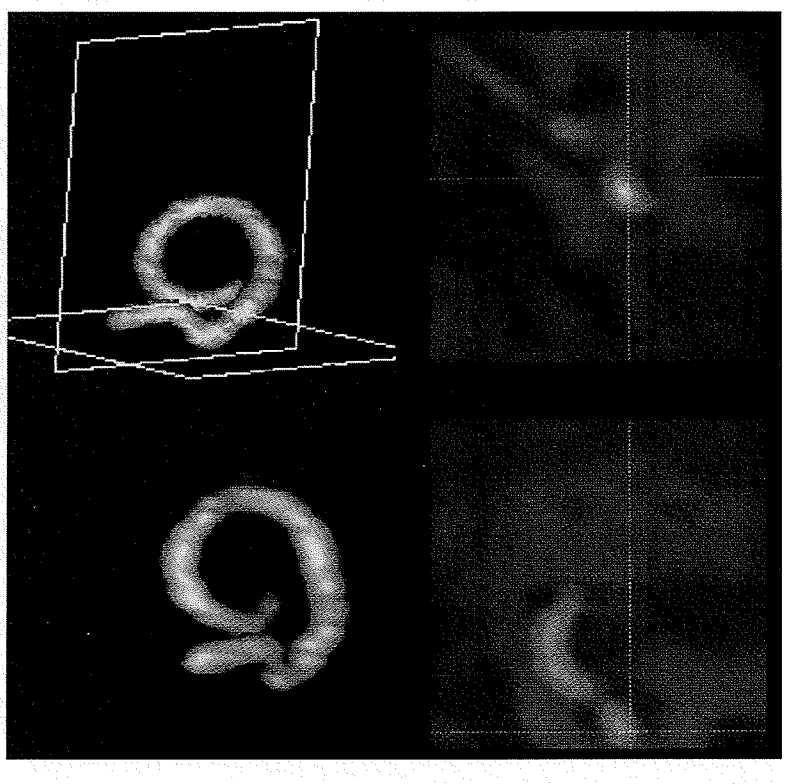

Fig 7. (Patient 16) Upper left panel has 2 rotations of 3-D reconstruction produced with ANALYZE that show implanted electrode array has 1.5 turns. This corresponds to 23 mm cochlear penetration, which is 79% of this individual's cochlear length. Reconstructions show array follows relatively straight path along drill track and has marked kink as array enters lower basal turn. This type of distortion, ie, recurve at entry to basal turn, was common finding in this group of patients, but it is unclear whether this is common among implant patients in general or if it is related to this surgeon's technique. Other panels show 2-D images reformatted along each of planes marked in upper left 3-D reconstruction.

Fig 8. (Patient 6) Reconstruction of this array obtained with Siemens 3-D software shows extreme case of multiple array distortions, including doubling, twisting, and accordion-like compressions. Arrows point to folds and intracochlear twists coincident with diminished function on electrodes 2 through 6 and electrodes 7 through 9.

mm) was longer than that for female patients (32.78 mm), but the groups were not significantly different according to the 2-tailed, equal variance Student's *t*-distribution statistic ($t = .48$).

Observations of Implanted Array Position in Cochlear Canal. Table 5 summarizes observations of electrode array position within the cochlear canal based on visual assessments of 2-D high-resolution postoperative scans for each patient. In 7 patients, the array enters the cochlea in the lower basal turn following a straight surgical drill track, but there is substantial variability in both the angle and entry point with respect to the basal turn. Cochlear entry points occurred in the lower to midbasal turn and in the hook region, and in some patients a parallel canal was formed nearly tangential to the first, which resulted in array entries up to 7 mm beyond the hook. Several patients had a distinct bend in the array just after it entered the scala tympani. Other patients had a kink (patients 2, 3, 6), twist (12, 14), or crimp (11, 13) in the lower to midbasal turn (Figs 6-8). The arrays of 10 patients impacted the outer bony wall of the cochlea in the middle to upper basal turn. Five patients had a distinct curve in the array in the upper basal turn, where the implant abutted the outer cochlear wall consistent with a shift from the scala tympani into the area equivalent to the scala media or scala vestibuli. Five patients had arrays that extended three quarters of a turn or less (Figs 6 and 8), while 4 had arrays that extended more than 1.25 turns (Fig 7).

Insertion Depth of Electrode Array. Insertion depths of patient electrode arrays estimated by Ketten using spiral calculations (K), by Wang using tracking and unwrapping (W), and by surgical observations (S) are listed in Table 4.

Comparison of CT-Based Estimates. There is excellent agreement across subjects between the two CT-based estimates of insertion depth ($r = .951$). Average insertion depths estimated by both methods are nearly 20% shorter (4 mm) than the anticipated full array insertion depth of 24 mm. Ketten's average estimate (20.19) was 0.17 mm less than Wang's (20.36 mm). This difference is approximately one half the length of an electrode band and less than the in-plane resolution of the spiral CT scan (0.35 mm). Ketten's and Wang's estimates of insertion depth differ by less than 0.4 mm for 7 patients, by 0.7 mm in 4 other patients, and by less than 1.5 mm in 8 patients. These numbers are equivalent to the scan resolutions and to 1 to 2 interelectrode lengths, respectively. The single largest difference is for patient 6, for whom Wang's estimate was 1.85 mm longer than estimates from Ketten or surgical observations. This was also the only patient with a noted surgical complication: the array was inserted, drawn out, and reinserted, producing marked crimping, twisting, and multiple, deep folds (Fig 8). For this patient, Wang reassessed the unwrap length by dividing the array into 4 parts for separate tracking and used a cubic spline interpolation along the center of mass of the array. Both iterations returned essentially similar lengths. The difference between Wang's and Ketten's estimates in this case is most likely related to inconsistencies in entry points, compounded by the tortuous shape of the array and a large metallic artifact in the middle ear and along the drill track.

The psychophysical data for patient 6 are consis-

tent with specific distortion points graphically visualized in the 3-D reconstruction of this array. Subarray spiral length calculations based on Ketten's method and assuming a 0.75-mm interelectrode spacing concluded the array's major twist occurred at electrodes 7 through 9. Patient 6 does not detect sounds on electrode 9, due to an electrical short in the lead wire, and he reports aberrant sound on electrodes 7 and 8. In addition, he has much slower than normal growth of loudness on electrodes 2 through 6, where there are distinct folds in the array.

The difference between Ketten's and Wang's estimates was greater than 1 mm for 6 other patients. Wang's estimates were longer for patients 3, 19, and 20. For patient 3, the implanted array had a noticeable bump in the lower basal turn that Wang's method followed. The actual insertion depth in the cochlear canal was probably slightly less, as reflected by Ketten's estimate. For patients 19 and 20, it was difficult to determine the entry points, because related anatomy was poorly defined. Consequently, as for patient 6, the entry points identified in the ANALYZE images for the unwrapping procedure may have differed from those used by Ketten. Ketten's estimates were longer than Wang's estimates for patients 7 and 9. Reasons for these differences are unresolved, but it is notable that these are the only 2 patients in whom the array appeared to distinctly follow the hook rather than a straight entry track (Table 5). Entry points chosen by Ketten for the spiral calculation incorporated portions of the hook that may not have been included in the unwrapping process. This suggests that the major source of discrepancies between the CT-based methods stems from subjective determinations of an entry point.

CT-Based Estimates Versus Surgeons' Observations. Ketten's and Wang's insertion depths were on average 0.75 mm shorter than the lengths estimated from the surgeon's observations (21.03 mm). This result was expected, because their CT-based estimates clearly reflect intracochlear array crimping or folding that intraoperative estimates cannot detect. Surgical estimates and those of Ketten and Wang were within 1.5 mm for 17 patients.

Detailed 3-D reconstructions of arrays clearly illustrate how the Nucleus electrode array can be distorted during surgical insertion and support Ketten's and Wang's shorter insertion depth estimates for most cases. The most extreme difference was for patient 11, for whom the surgical insertion depth estimate (20.25 mm) was more than 6 mm longer than that of either Ketten or Wang (13.68 and 14.10 mm, respectively). Figure 6 shows the extreme intracochlear compression of that implant. Patients 13 and 16 also had marked crimping of their arrays. Patient 4's array tunneled through the remains of a cochlear canal compromised by massive otosclerotic degeneration (Table 5). For each of these patients, the surgical estimate of insertion depth was approximately 1 mm longer than that of Ketten or Wang. Ketten's and Wang's estimates for patient 9 were also significantly shorter than the surgically observed length, implying it, too, was compressed. Specific distortions were not noted in the summary report (Table 5), but extensive bone and fibrous tissue were observed that may have masked a compression. For patient 17, the surgically derived estimate of insertion depth was 2.33 and 1.64 mm longer, respectively, than that of Ketten and Wang. In this case, substantial compression was clearly consistent with extensive bony deposits noted in the upper basal and lower middle turns. Given these data, most array compressions, including ones involving as much as 10% of the array length, are not detectable intraoperatively.

Estimates of Cochlear and Array Characteristic Frequency Distributions. For characteristic frequency estimates, both total cochlear length and the longitudinal position of the array are required. At present, the curvilinear tracking algorithm cannot measure cochlear length. Therefore, Ketten's estimates of canal length and array position were used for these calculations, because they were determined by a consistent technique. However, Wang's estimated insertion depth correlated with Ketten's, and either theoretically could be used for array length estimates.

Table 3 shows calculated cochlear canal length, percentage of cochlear canal length occupied by the implanted array, and estimated characteristic frequencies. Insertion depths vary widely among patients (range 13.68 to 24.46 mm), with a mean insertion depth of 20.19 mm. Although median array insertion depths are longer for male patients (21.2 mm) than female patients (20.7 mm), average percentages of cochlear canal length covered by the array are not significantly different (62% for male patients and 61% for female patients), and the distributions are isomorphic (ranges 47% to 79% for male patients and 46% to 74% for female patients).

Two characteristic frequency data sets were calculated from Greenwood's formulae. One is based on Greenwood's average human cochlear length of 35 mm; the other, on this group's mean of 33.01 mm. Estimates are given for the minimum and maximum frequencies of each patient's cochlea and for the characteristic frequency equivalent to the most apical electrode position in each patient's array.

Potential hearing ranges calculated for these ears with Greenwood's equations are consistent with the

typical human range of 20 Hz to 20 kHz. The average frequencies at the most apical electrode for the 35- versus 33.01-mm normalized data were 1,158 and 1,030 Hz, respectively. This is higher than expected from manufacturer's projections, but is consistent with an average insertion depth several millimeters short of optimum insertion. The large range of predicted apical electrode frequencies (435 to 2,919 Hz for the 35-mm normalized data; 387 to 2,596 Hz for the 33.01-mm normalized set) reflects the large interindividual differences in each implant's relative cochlear distribution (46% to 79%).

DISCUSSION

In any morphometric study, it is important to understand the sources and magnitudes of measurement error. Fundamental issues for calculating cochlear lengths from in vivo CT scans are 1) the resolution of the images, 2) the resolution of the measurement devices, and 3) the magnitude of cochlear canal deviations from the spiral model chosen for calculating arc length.

As stated earlier, true midmodiolar sections are important for accurate length estimates. Takagi and Sando[14] showed that when cochleae are cut obliquely, the measured length is significantly shorter. Because of the range and orientation of cochlear tilt in humans (approximately 7° and 14°, latero-inferior), most standard temporal bone CT views are slightly oblique to the modiolar spiral axis. For future studies, errors can be minimized by matching gantry tilts to each subject's modiolar axis a priori, but for retrospective studies like this one, reformatting para-modiolar images from 3-D reconstructions is a reasonable alternative. Because 3-D reconstructions can be rotated to any orientation, the subject's cochlea can be aligned to a standardized position for reformatting and measured in a specific, consistent plane. This is important for both comparative and longitudinal studies of cochlea-implant relationships. Reformatted images, depending on the degree of interpolation required, can have significantly lower resolutions than original scans; however, with 100 μm spiral scan reconstructed voxels, interpolated images have resolutions equivalent to those of the original scan images (Fig 4).

As indicated previously, reformatted images were required for all hook region measures. Because the optimal scan angle for the cochlea does not provide a clear in-plane view of the hook, it was not possible to measure the hook directly from a single image. We concluded that measuring hook lengths was warranted but not crucial for this study, because of the high characteristic frequencies of neurons in this region. Therefore, reformatted images were acceptable for primary measures of the length of the hook. This is, however, an area of the cochlea that warrants further attention to improve the accuracy of its measurement and our understanding of its variability.

In some patients, it is difficult to determine canal and modiolar axes because of osteogenic changes or capsular degeneration. In these cases, the error in measurement is dictated primarily by the error related to estimating the central axis of the cochlear canal with a regular spiral path.

An important limiting factor for electrode resolution in this study is derived from partial volume averaging effects in CT images. Pixel gray levels are determined by the averaged attenuation of structures within the object volume the pixel represents. Exceptionally dense structures, eg, electrodes or even hypermineralized foci in otosclerotic ears, may appear larger in CT images than they are, through "blooming." Dense material may occupy only a small percentage of an imaged volume, but if its attenuation is high enough, its value drives the volume average to the maximum. Hence, the edge of the object "blooms," because the entire affected pixel is imaged at the maximum gray level. Skinner et al[33] found the bloom is spherical for implanted arrays and, on average, triples the array's apparent cross section. Because path lengths are based on the central axis of the array, partial volume averaging effects will not introduce significant errors in length calculations except at the entry and tip regions. The entry point is dictated, in part, by anatomic features; therefore, partial volume effects potentially have the greatest impact on tip identification. If profiling is used to counteract blooming, the estimated error in apical electrode position is on the order of the spiral scan elements, ie, ±0.1 mm.

Few implants in this study paralleled the curvature of the cochlear canal, and one third did not remain in the scala tympani (Table 5). Most had a regular curvature but a different planar axis than the basal turn. These implant lengths could be accurately calculated, because the array's axial height and radii were measured separately. For implants with significant kinks, compressions, or twists in the array, the path was calculated with multiple spline fits. We have no metric for determining the error inherent in these cases. An additional complication in several cases was that the center of the array path could not be reliably determined at points where the array impacted the bony wall of the cochlea. As indicated in the Methods section, if preoperative scans are available, the subtractive method for calculating implant insertion depth is potentially more robust.

The unwrapping algorithm is designed to track the center of mass of a curvilinear structure in predetermined, small steps. If the dimensions of kinks, folds, or twists in the array are comparable to the tracking step, the algorithm may compute a convoluted path unrelated to cochlear penetration. In this case, the estimated insertion depth will be longer than the functional length estimated by the morphometric method.

Scan resolutions are the largest quantifiable error for the CT-based estimates employed in this study. Repeatability of arbitrarily selected measurement points on a reconstructed image differed by ≤2 pixels for most patients, but were as high as 3 pixels for some. A spread of ±3 pixels has an associated error of ±0.35 mm, ie, equivalent to standard in-plane resolutions.

The principal source of error in insertion depth estimates from surgical observations is that all inserted electrodes are presumed to be evenly distributed throughout the cochlear canal. Because twists and compressions cannot be readily detected intraoperatively, overestimates of functional length are likely. It is not possible to provide a meaningful average error based on this study; the data show that for any given individual, the specific error can be substantial.

With these caveats, how do the three measures of arrays compare? The insertion depths estimated by Ketten, Wang, and the surgeons for patients 2, 5, 8, and 14 were within 0.36 mm of each other. This is consistent with the in-plane resolution of the spiral CT scans (0.35 mm) and with the findings of Skinner et al[33] for electrode resolution. The small average difference between Ketten's and Wang's estimates of insertion depth (0.17 mm) is also consistent with differences on the order of scan image resolutions. Setting aside image limitations, one possible reason Ketten's estimates are on average shorter than Wang's is that Wang's method follows the center of mass of the array, incorporating kinks and bends into the length, whereas Ketten's method purposely estimates a functional insertion in the context of preoperative cochlear canal length.

Where the surgeon's estimate is longer than both Ketten's and Wang's estimates, the differences are consistent with the conclusion, reinforced by 3-D visualizations, that there was substantial compression of the array. It is likely the array distortions occurred during insertion but were undetected. The most striking example of this is patient 16. For patient 11, the attenuated insertion depth estimate is underscored by the correlation between the morphometric and performance data. Although assessing array distortion was not an intended focus of this study, it is important to note that moderate to extensive intracochlear compressions of the array were observed in the CT reconstructions of implants for nearly one third of the patients in this study. Our study population may not be representative of the implant population for a variety of reasons, but the incidence and range of array deformations detected in this study argue strongly for high-resolution postoperative CT examinations of any implant recipient with aberrant or diminished performance following an otherwise "normal" implantation procedure.

For the 20 patients in this study, the mean cochlear canal length of 33.01 mm is shorter than that chosen by Greenwood for his most recent calculation of cochlear frequency-position function,[22] but is close to values reported in other studies.[10,11,13,14] The range of cochlear canal lengths (29.07 to 37.45 mm) also agrees well with data from normal and implanted human temporal bones.[10-17] We found a slightly longer mean cochlear canal length in male patients (33.45 mm) than in female patients (32.80 mm) that was not statistically significant, in contrast to the data of Sato et al,[13] who reported a significant difference between male (37.1 ± 1.6 mm) and female (32.3 ± 1.8 mm) cochlear lengths. It should be noted, however, that while our subject population is large enough for determining general trends, our male-female distribution is not sufficient for analyzing gender-dependent differences.

It is remarkable that while the mean surgical insertion depth is approximately 61% of cochlear canal length, the range is 46% to 79%. Considering that these patients were all reported to have a full insertion of 22 electrodes, the 3- to 4-octave range difference in predicted apical electrode frequencies (435 to 2,919 Hz for the 35-mm normalized data; 387 to 2,596 Hz for the 33.01-mm normalized set) is striking and clearly has important clinical implications. Although the majority of patients could be fitted with a characteristic frequency mapping procedure like that of Whitford et al[7] and Eyles et al,[8] some patients, eg, 6, 10, 11, and 14, do not have sufficient electrodes apical to the 3,000-Hz point to carry first and second formant speech information. Skinner et al[5,6] showed the importance of having multiple electrodes assigned to first formant frequencies at or below 1,000 Hz to improve recognition of phonemic cues, words, and sentences in noise. It appears that implant recipients recognize speech cues through different stimulations at multiple electrodes, even if the signal frequency mapping does not necessarily match the probable characteristic frequencies of the electrodes involved. The challenge for future research is to determine what is the optimal balance of mapping for differentiable percepts versus character-

istic frequencies of the nearest neurons.

Earlier 2-D methodologies for quantifying intracochlear relationships of implant electrodes, eg, those of Marsh et al[29] and Cohen et al,[30] are important steps toward the common goal of functional frequency maps. Advantages to their procedures are that the resolution of individual electrodes is very good, the costs are relatively low, and the facilities are widely available. Disadvantages to these 2-D X-ray approaches are that it is difficult to obtain a true axial projection and that cochlear anatomic and array details are often masked by superimposed structures. Two-dimensional measures necessarily underestimate length, because even if the X-ray projection parallels the cochlear axis, the height of the cochlea is not taken into account. Off-axis projections further compromise the accuracy of 2-D calculations,[13,19] and because consistent angles are difficult to obtain, both interpatient and, over time, intrapatient comparisons are problematic. Finally, without multiple single-plane X-rays taken at different angles, it is generally not possible to determine unimplanted cochlear lengths or quantify distortions in the array. An important aspect of the work by Cohen et al[30] is that the template they devised can be used in a relatively straightforward manner for clinical assessments of array-frequency distributions. However, it assumes there is a direct correspondence between angular position and characteristic frequency that has not been demonstrated. In fact, the characteristic frequency estimators used by Cohen et al to derive the template are largely length-based and were primarily designed to calculate length-dependent differences in critical band distributions and overall frequency ranges.[20,21,23]

In summary, conventional 2-D radiographic techniques provide good, relatively rapid first-order approximations of array insertion depth, but they cannot tap the rich information on individual patient anatomy and implant relationships implicit in spiral CT scan data. Nor can they approach the accuracy of measures and comparisons obtainable with ultrahigh resolution 3-D cochlear reconstructions.

This paper demonstrates the current potential and limits of clinical level imaging technologies to measure cochlear canal and implanted electrode array features that are important for developing patient-specific frequency maps. To locate each electrode in the spiral CT scan images still requires interactive profiling of individual scans and reconstructions. Recent technologic advances in submillimeter collimation, table movement, and deblurring algorithms hold promise for enhanced, automated electrode segmentations and measurement. These advances will ultimately improve our understanding of the intricate, 3-D complexity of the temporal bone and thus lead to better surgical approaches, more accurate electrical field models, and advances in electrode designs. At this time, our existing tools have barely been exploited, but they can clearly provide important keys for optimizing and individualizing coding strategies and fitting procedures that may enhance every patient's capacity to utilize sound.

ACKNOWLEDGMENTS — Every paper is a composite of its authors' efforts. Although it is not possible to have more than one first author, on several counts, Dr Skinner deserves to share that designation. The authors are indebted to Siemens for access to the submillimeter and scale expansion software for reconstruction of Somatom PLUS S spiral computed tomography data and to Dr Richard Robb of the Mayo Clinic for access to the ANALYZE software. These were valuable tools for this project. We are grateful to Barry Brunsden, Robert Knapp, RT(R), Roberta L. Yoffie, RT(R), and Glenn J. Foster, RT(R), for their technical assistance and to radiologic technologists (RT[R]) Christine Block, Barbara Blocker, Jeff Dalton, Dareld LaBeau, Joan Laughhun, Michael Ritter, Terry Shelby, Cathy Valenza, Julie Arruda, and Ann McDermott for their expertise in obtaining and processing preoperative and postoperative spiral computed tomography patient data. Gary Harding, Timothy Holden, and Scott Cramer provided helpful critiques and assistance in the preparation of this manuscript. We also thank two anonymous reviewers who provided helpful suggestions and extremely valuable reviews of our data.

REFERENCES

1. Blamey PJ, Pyman BC, Gordon M, et al. Factors predicting postoperative sentence scores in postlinguistically deaf adult cochlear implant patients. Ann Otol Rhinol Laryngol 1992; 101:342-8.

2. McKay CM, McDermott HJ, Vandali AE, Clark GM. The Spectral Maxima Sound Processor: recent findings in speech perception and psychophysics. In: Hochmair-Desoyer IJ, Hochmair ES, eds. Advances in cochlear implants. Vienna, Austria: Manz, 1993:141-6.

3. Miyamoto RT, Maddox HE III. Medical and surgical issues. Am J Otol 1991;12(suppl):18-21.

4. Finley CC, Wilson BS, White MW. Models of neural responsiveness to electrical stimulation. In: Miller JM, Spelman FA, eds. Cochlear implants: models of the electrically stimulated ear. New York, NY: Springer-Verlag, 1989:55-93.

5. Skinner MW, Holden LK, Holden TA. Effect of frequency boundary assignment on speech recognition with the Speak speech-coding strategy. Ann Otol Rhinol Laryngol Suppl 1995; 104(suppl 166):307-11.

6. Skinner MW, Holden LK, Holden TA. Parameter selection to optimize speech recognition with the Nucleus implant. Otolaryngol Head Neck Surg 1997;117:188-95.

7. Whitford LA, Seligman PM, Blamey PJ, McDermott HJ, Patrick JF. Comparison of current speech coding strategies. Adv Otorhinolaryngol 1993;48:85-90.

8. Eyles JA, Boyle PJ, Burton MJ. Characteristic frequency mapping in subjects using the Nucleus 22-channel cochlear implant system with partial and full insertion. Ann Otol Rhinol Laryngol Suppl 1995;104(suppl 166):356-8.

9. Rosen S. Electrode placements for cochlear implants: a

review. Br J Audiol 1990;24:411-8.

10. Ulehlova L, Voldrich L, Janisch R. Correlative study of sensory cell density and cochlear length in humans. Hear Res 1987;28:149-51.

11. Hardy M. The length of the organ of Corti in man. Am J Anat 1938;62:291-311.

12. Bredberg G. Cellular pattern and nerve supply of human organ of Corti. Acta Otolaryngol [Suppl] (Stockh) 1968(suppl 236).

13. Sato H, Sando I, Takahashi H. Sexual dimorphism and development of the human cochlea: computer 3-D measurement. Acta Otolaryngol (Stockh) 1991;111:1037-40.

14. Takagi A, Sando I. Computer-aided three-dimensional reconstruction: a method of measuring temporal bone structures including the length of the cochlea. Ann Otol Rhinol Laryngol 1989;98:515-22.

15. Nadol JB Jr, Young Y-S, Glynn RJ. Survival of spiral ganglion cells in profound sensorineural hearing loss: implications for cochlear implantation. Ann Otol Rhinol Laryngol 1989; 98:411-6.

16. Linthicum FH, Fayad J, Otto SR, Galey FR, House WF. Cochlear implant histopathology. Am J Otol 1991;12:245-311.

17. Nadol JB Jr, Ketten DR, Burgess B. Otopathology in a case of cochlear implantation. Laryngoscope 1994;104:299-303.

18. O'Reilly BF. Probability of trauma and reliability of placement of a 20 mm long model human scala tympani multielectrode array. Ann Otol Rhinol Laryngol Suppl 1981;90(suppl 82):11-2.

19. von Békésy G . Experiments in hearing. New York, NY: McGraw-Hill, 1960.

20. Greenwood DD. A cochlear frequency-position function of several species — 29 years later. J Acoust Soc Am 1990;87: 2592-605.

21. Greenwood DD. Critical bandwidth and the frequency coordinates of the basilar membrane. J Acoust Soc Am 1961;33: 1344-56.

22. Greenwood DD. Approximate calculation of the dimensions of traveling-wave envelopes in four species. J Acoust Soc Am 1962;34:1364-9.

23. Greenwood DD, Joris PX. Mechanical and "temporal" filtering as codeterminants of the response by cat primary fibers to amplitude-modulated signals. J Acoust Soc Am 1996; 99:1029-39.

24. Fay RR. Structure and function in sound discrimination among vertebrates. In: Webster DB, Fay RR, Popper AN, eds. The evolutionary biology of hearing. New York, NY: Springer-Verlag, 1992:229-63.

25. Allen JB, Neely ST. Micromechanical models of the cochlea. Physics Today 1992;45:40-7.

26. Ketten DR, Wartzok D. Three-dimensional reconstructions of the dolphin ear. In: Thomas J, Kastelein R, eds. Sensory abilities of cetaceans. New York, NY: Plenum Press, 1990: 81-105.

27. Ketten DR. The marine mammal ear: specializations for aquatic audition and echolocation. In: Webster D, Fay RR, Popper AN, eds. The evolutionary biology of hearing. New York, NY: Springer-Verlag, 1992:717-54.

28. Echteler SW, Fay RR, Popper AN. Structure of the mammalian cochlea. In: Fay RR, Popper AN, eds. Comparative hearing: mammals. New York, NY: Springer-Verlag, 1994:134-71.

29. Marsh MA, Xu J, Blamey PJ, et al. Radiologic evaluation of multichannel intracochlear implant insertion depth. Am J Otol 1993;14:386-91.

30. Cohen LT, Xu J, Xu SA, Clark GM. Improved and simplified methods for specifying positions of the electrode bands of a cochlear implant array. Am J Otol 1996;17:859-65.

31. Ketten DR. The role of temporal bone imaging in cochlear implants. Curr Opin Otolaryngol Head Neck Surg 1994;2: 401-8.

32. Wang G, Vannier MW. Longitudinal resolution in volumetric X-ray computerized tomography: analytical comparison between conventional and helical computerized tomography. Med Phys 1994;21:429-33.

33. Skinner MW, Ketten DR, Vannier MW, Gates GA, Yoffie RL, Kalender WA. Determination of the position of Nucleus cochlear implant electrodes in the inner ear. Am J Otol 1994; 15:644-51.

34. Seicshnaydre MA, Johnson MH, Hasenstab MS, Williams JH. Cochlear implants in children: reliability of computed tomography. Otolaryngol Head Neck Surg 1992;107:410-7.

35. Klein H, Bohndorf K, Hermes H, Schutz W, Gunther R, Schlondorff G. Computed tomography and magnetic resonance imaging in the preoperative work-up for cochlear implant. Eur J Radiol 1992;15:817-24.

36. Kalender WA. Thin-section three-dimensional spiral CT: is isotropic imaging possible? Radiology 1995;197:578-80.

37. Kalender WA, Seissler W, Klotz E, Vock P. Spiral volumetric CT with single-breath-hold technique, continuous transport, and continuous scanner rotation. Radiology 1990;176:181-3.

38. Kalender WA, Polacin A, Suss C. A comparison of conventional and spiral CT: an experimental study on detection of spherical lesions. J Comput Assist Tomogr 1994;18:167-76.

39. Ketten DR, Nadol JB Jr. Imaging and temporal bone diagnostics in cochlear implantation [Abstract]. Second International Cochlear Implant Symposium, Iowa City, Iowa, 1990.

40. Robb RA. ANALYZE Reference Manual, Version 6.2, Biomedical Imaging Resource. Rochester, Minn: Mayo Foundation, 1993.

41. Wang G, Vannier MW, Skinner MW, Kalender WA, Polacin A, Ketten DR. Unwrapping cochlear implants by spiral CT. IEEE Trans Biomed Eng 1996;43:891-900.